J Mater Sci (2015) 50:5276–5285
DOI 10.1007/s10853-015-9075-0

Importance of interfacial step alignment in hetero-epitaxy and orientation relationships: the case of Ag equilibrated on Ni substrates. Part 2 experiments

Dominique Chatain[1] · Paul Wynblatt[2] · Anthony D. Rollett[2] · Gregory S. Rohrer[2]

Received: 6 January 2015 / Accepted: 30 April 2015 / Published online: 15 May 2015

Abstract The orientation relationships (ORs) that develop when Ag films are equilibrated on more than 200 different Ni substrate orientations distributed over the standard stereographic triangle have been determined by electron backscatter diffraction. Four different types of OR have been observed, including cube-on-cube, twin-related, oct-cube (that develops only on Ni(100)), as well as a family of more complex ORs (referred to as "special") that arise during the gradual transition from the oct-cube to the twin OR. The importance of the alignment of step edges on the Ag side of the interface with those of the Ni substrate, in the development of ORs, has been validated by comparison with the results obtained on the large range of substrate orientations investigated in this study. This step alignment occurs in the early stages of film formation, but is also consistent with equilibrium ORs as it tends to produce minimum energy interfaces. This feature of hetero-epitaxy and of the resulting ORs has not previously been emphasized.

✉ Dominique Chatain
chatain@cinam.univ-mrs.fr

Paul Wynblatt
pw01@andrew.cmu.edu

Anthony D. Rollett
rollett@andrew.cmu.edu

Gregory S. Rohrer
gr20@andrew.cmu.edu

[1] Aix-Marseille Université, CNRS, CINaM, UMR 7325, 13288 Marseille, France

[2] Department of Materials Science and Engineering, Carnegie Mellon University, Pittsburgh, PA 15213, USA

Introduction

The purpose of this paper is to determine the origins of the orientation relationships (ORs) obtained by equilibrating a deposit of one face-centered cubic (FCC) metal on a substrate of a different FCC metal. The literature contains reports of experimental and modeling studies of several such FCC A-on-B systems, including Ag on Ni [1–16], Ni on Ag [17], Au on Cu [11], Pb on Cu [18], and Pb on Ni [19]. Thus far, experimental investigations have focused on B-substrates with low-index surfaces oriented along (111) and (100) crystallographic planes. Detailed studies of B-substrates with a (110) surface orientation have also been reported for Ag on Ni [5, 6, 11, 12]. Both experiments and computer simulations have been performed and compared on these three low-index substrate orientations. It is important to mention that previous experiments have been performed by two different approaches, either by "hetero-epitaxial" growth or by the particle rotation method [20].

Literature reports indicate that on these low-index substrate orientations, the most important parameter for determining the resulting OR is the difference in atomic size between the A and B species. When the A species is equilibrated on B(111), it adopts an OR in which A{111}// B(111), with either a cube-on-cube or a twin-related OR [6]. In contrast, on B(100), either a cube-on-cube OR with A(100)//B(100), or a so-called oct-cube OR with A(111)// B(100), has been reported [6, 13]. Furthermore, the results of some simulations have indicated that the oct-cube OR is more likely when the atomic size of the A-component is much larger than that of the B-component [17]. For Ag on a Ni (110) substrate, Allameh et al. [11] report a cube-on-cube OR.

We have chosen to investigate the Ag–Ni system because of the negligible mutual solubility of these

components. Also, since the lattice parameter of Ag is larger than that of Ni by about 16 %, it is expected that the observed ORs will reflect the effects of lattice mismatch. One important difference between the present work and that of previous studies is that we have equilibrated Ag on a polycrystalline Ni substrate in order to investigate the ORs that develop on a large number of Ni surface orientations, spanning all distinguishable orientations. Finally, it is important to mention that in parallel with this experimental study, molecular dynamics computer simulations of Ag equilibrated on Ni substrates of various orientations have been performed. These are reported in the companion paper [21] and have been very useful in pointing to step alignment as an important feature of OR development that has not previously been emphasized.

Experimental procedures

Polycrystalline Ni substrates with grains of surface orientations spanning the range of distinguishable orientations were prepared as follows. Samples with dimensions of about 8 × 5 mm were produced by cold-rolling a 3-mm diameter 99.999 % pure Ni rod to 1 mm in thickness. They were then polished with an alumina slurry down to 0.1 μm, and recrystallized in a horizontal silica-tube furnace for 2 h, at 1023 K, under a flow of Ar + 5 % H_2. Such annealing produces Ni grains which range in size from 10 to 100 μm, and have no significant orientation texture. Larger grains could be obtained by longer annealing, but the sample surface then developed a strong (100) texture that was not convenient for the purposes of our experiment. Ni substrates with the greatest variety of grain surface orientations were transferred to a vacuum chamber operated at a pressure of 10^{-8} Pa for Ag deposition by e-beam evaporation from a 99.99 % pure target. The Ni sample was first annealed at 400 ± 20 K for 1.5 h, in situ, and then a 25-nm thick Ag film was deposited on its surface at ~413 K.

The orientations of the substrate Ni grains and of the deposited Ag grains were determined by electron backscatter diffraction (EBSD). Automated EBSD mapping was performed in a FEI Quanta 200 FE ESEM equipped with an EDAX/TSL orientation system and a Hikari high speed EBSD detector. The data were collected at 20 kV at a sample tilt of 70° relative to normal incidence of the electron beam, at a working distance of 10 mm. All the data were processed with the OIM-TSL software. Figure 1 presents typical maps of the same region of the polycrystalline Ni sample before and after Ag deposition. These maps are inverse pole figures (IPFs) in the (001) and (010) directions of the reference frame of the microscope, which are in the surface normal and in an in-plane direction of the substrate, respectively. The color code is given in the standard stereographic triangle (SST) to the right of Fig. 1. The two IPF maps of the film show that the shapes displayed by the features of the Ag deposit match those of the Ni, grain by grain. This indicates that all the Ag grains of the film located on a given Ni grain have essentially the same orientation. However, they contain defects which appear as pixels of different colors. Actually, as shown in Fig. 2a, the Ag film on each Ni grain is neither flat nor continuous. Rather, it consists of facetted nano-grains with sizes ranging from 50 to 300 nm. Such a microstructure explains the defects in the IPFs of the Ag film that is apparent in the Ag maps of Fig. 1.

While the Ag grains of the film seem to be already well oriented on each of the Ni grain surfaces in Fig. 1, the OR between Ni and Ag cannot precisely be determined from such images. This is because there is a small misorientation between the sample before and after Ag deposition that occurs when the sample is remounted on the microscope stage. In order to measure the Ag and the Ni orientations simultaneously and thus determine the orientation relationship with maximum accuracy, well-dispersed Ag particles on Ni grains were produced by annealing the sample at 923 K for 2 h under an Ar + 5 %H_2 flow in the silica-tube furnace, as previously done for the Cu/sapphire system [22]. Annealing produces Ag particles ranging in size from 500 nm to 1 micron, depending on the Ni grain surface orientation as shown in Fig. 2b. The Ag particles consist predominantly of faceted single crystals, although some twinned Ag polycrystals are also observed. In such samples, the Ag particles and the Ag-free Ni surfaces between them are large enough for their orientations to be determined simultaneously by EBSD.

Figure 3a presents a secondary electron image that shows a region with Ag crystals on nine Ni grains. An IPF(001) map of six of these Ni grains with their Ag crystals is shown in Fig. 3b. The black regions of this map are unidentifiable because of shadowing by the Ag crystals [18, 22]. The ORs of Ag on more than 200 Ni grains were acquired during several EBSD sessions, separated by sample removal from the microscope. In order to correct for any misalignment of the sample between two sessions, each dataset included one Ni(100) grain (i.e., with a (100) surface plane) which was used as a reference for realigning the sample z-direction of the microscope with the [100] direction of this Ni grain. Ni(100) grains can easily be recognized by the meandering finger-like shape of their Ag crystals, as seen in Fig. 3b.

A semi-quantitative comparison of some of the orientation data of the Ag film deposited at ~413 K (from figures such as Fig. 1) and of the Ag crystals obtained after annealing at 923 K (from figures such as Fig. 3) does not reveal any significant changes in the Ag orientation from

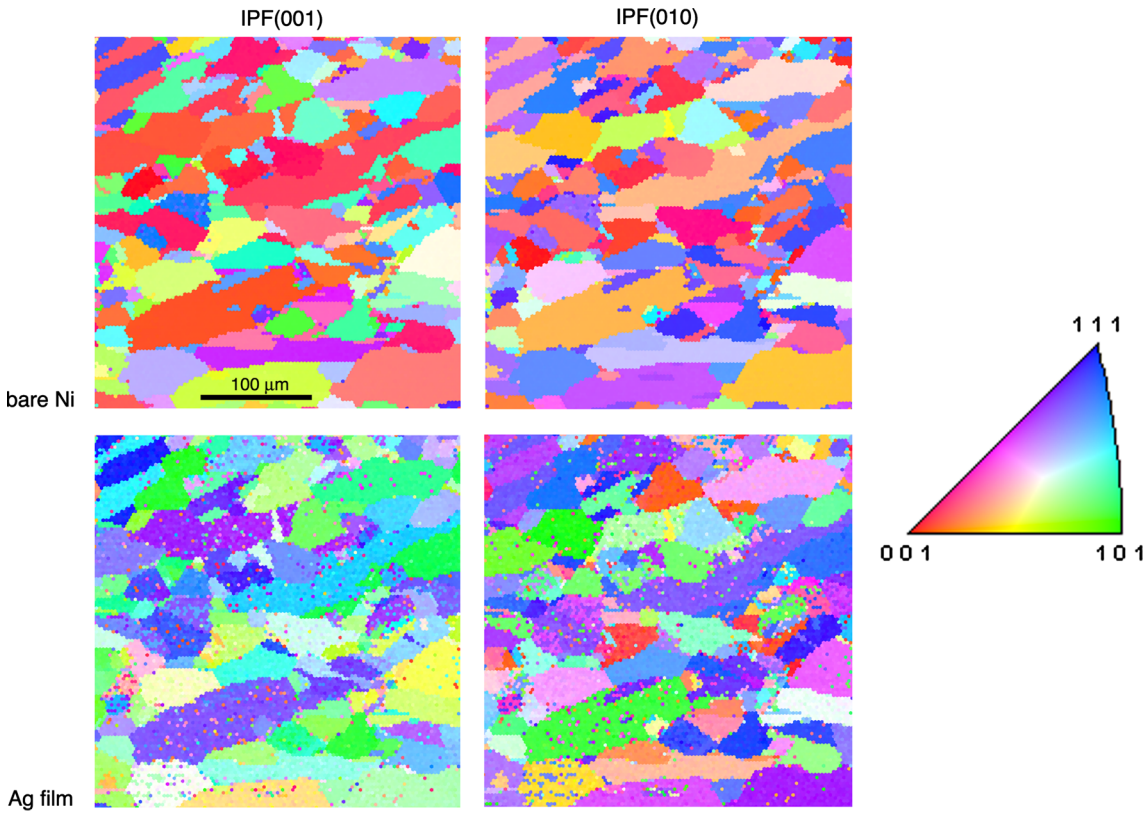

Fig. 1 Inverse pole figure (IPF) maps of grains of the same region of a sample in two perpendicular directions of the microscope reference frame. The *top panels* correspond to the bare Ni substrate, and the *bottom panels* to the Ag deposit on Ni; the orientation color code is given in the SST on the *right* (Color figure online)

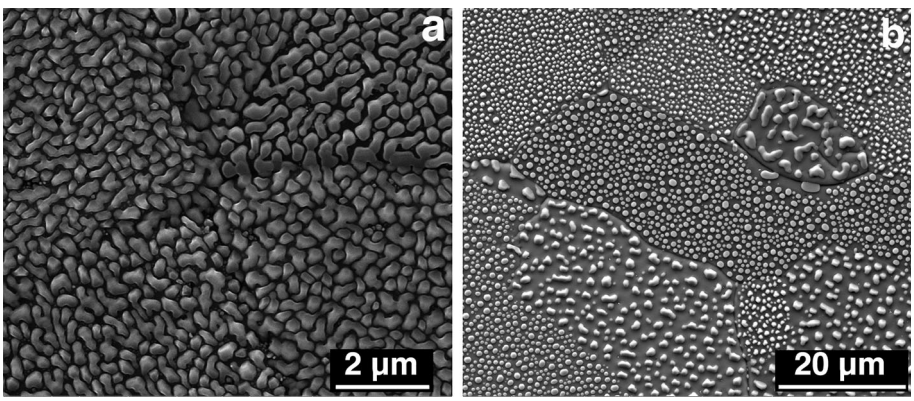

Fig. 2 **a** SEM micrograph of Ag film microstructure after deposition at 413 K. Top view of five grains. **b** SEM micrograph of Ag crystals on the Ni grains after annealing at 923 K for 2 h. Note the different dispersions and sizes of Ag crystals residing on Ni grains of different orientations

the annealing process, within the misalignment error that results from sample repositioning in the EBSD-SEM. This means that the Ag deposition at ~400 K already produces Ag grains with an equilibrated OR, and that the annealing treatment does not significantly change the OR of Ag on Ni.

The experimental error on the absolute orientation of the Ni surface is estimated to be of the order of ±3°, while the error on the orientation relationship between the Ag film and the Ni substrate is expected to be less than ±0.5°.

Results

General picture of OR distribution

The ORs of the Ag crystals on each Ni(*hkl*) grain were determined from the EBSD patterns of Ni and Ag, and the corresponding Euler angles provided by the OIM-TSL software. Figure 4a summarizes the overall picture of the distribution of the preferred ORs in the form of a SST which displays the ~200 Ni substrate orientations for

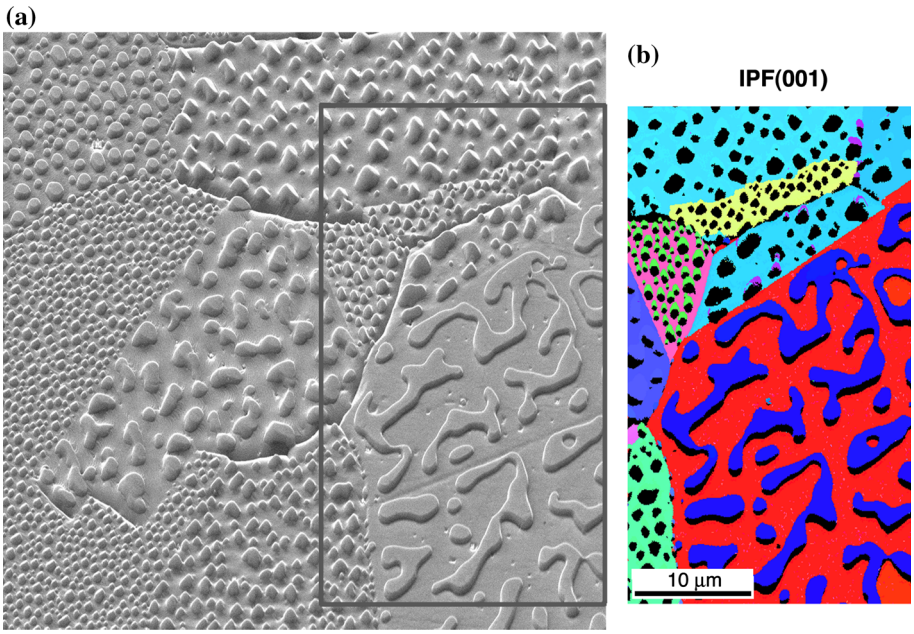

Fig. 3 **a** Secondary electron image of a region with nine Ni grains and their associated Ag crystals. This image has been corrected for sample tilt in the microscope. **b** Orientation map of the outlined portion of (**a**). At the bottom right, a Ni(100) grain (*red*) can be recognized by its meandering finger-like Ag(111) crystals (*blue*). On most of the other Ni grains, the color of the Ag crystals is close to that of the underlying Ni grain, and the *black* regions next to each Ag grain are unidentifiable because of shadowing by the Ag crystals due to sample tilt [18, 22] (Color figure online)

which the Ag ORs were determined. In this SST, the dashed line represents the $[1\bar{2}1]$ zone which connects the (210) and (111) planes. Four principal ORs were observed:

(1) A cube-on-cube OR, which will be referred to as OR(C), is displayed by Ag on the Ni surfaces with orientations that lie in the (210)–(111)–(110) portion of the SST. The corresponding Ni substrate orientations are shown as purple points in Fig. 4a. OR(C) may be expressed as $Ag(100)[01\bar{1}]//Ni(100)[01\bar{1}]$.

(2) A twin OR, which will be referred to as OR(T), appears with an approximately equal frequency to the OR(C) for the Ni substrate orientations that lie close to the $[1\bar{2}1]$ zone. They correspond to the light blue points in Fig. 4a. OR(T) may be expressed as $Ag(11\bar{1})[1\bar{1}0]//Ni(111)[01\bar{1}]$.

(3) An oct-cube OR, which will be referred to as OR(O), is only adopted by Ag on Ni(100), and is displayed as a green point in Fig. 4a. This OR may be expressed as $Ag(111)[1\bar{1}0]//Ni(100)[01\bar{1}]$.

(4) A family of special ORs, which will be referred to as OR(S), arises as the result of a gradual transition from OR(O) to OR(T). These ORs are adopted by Ag on Ni substrate orientations that lie within the (100)–(111)–(210) triangle (blue points in Fig. 4a). As we shall see later, the Ag orientations that correspond to OR(S) fall within the (111)–(110)–(210) region of the SST that is distinct from the orientation space occupied by the Ni substrates.

Details on the observed ORs

In order to give a pictorial representation of the four kinds of observed ORs, Fig. 4b presents twelve pole figures (PFs) which compare the locations of the ⟨110⟩ poles of Ni and Ag. Only the poles in the northern hemisphere are displayed. Each of these PFs, labeled by the Ni(*hkl*) substrate surface plane, displays the ⟨110⟩ poles of the Ni(*hkl*) grain (blue round symbols) and the ⟨110⟩ poles of the corresponding Ag crystals (square symbols). The square symbols may be of different colors when they refer to different Ag ORs. Red square symbols correspond to the preferred (most frequent) OR.

One notable result is that, independent of the orientation of the Ni(*hkl*) substrate grain, at least one of its ⟨110⟩ poles lies very close to a ⟨110⟩ pole of each Ag crystal on that Ni surface. Furthermore, these close-to-coincident ⟨110⟩ orientations lie systematically either on the outer circle of the PF or close to it, i.e., they either lie in, or close to, the plane of the Ni/Ag interface. When coincident poles lie on the outer circle of the PF they may appear twice at diametrically opposite locations, the second appearance representing the inverse direction of the first. Those occurrences have been highlighted in the PFs of Fig. 4b by enclosure within a red circle. If the coincident poles lie within the outer circle of the PF, then the inverse direction lies in the southern hemisphere, and is not plotted; however, we have marked the location of the inverse pole by an empty red circle. A computer program was used to calculate the smallest angle, γ, between all possible ⟨110⟩ directions of a Ni(*hkl*) grain and those of its associated Ag crystals, from the Euler angle data recorded during the EBSD experiments [23]. The average value of γ for the Ag crystals lying on $\sim$200 Ni grains, distributed throughout the SST, is $0.85° \pm 0.8°$. A similar result was observed in the simulations reported in the companion paper [21], although the coincidence between

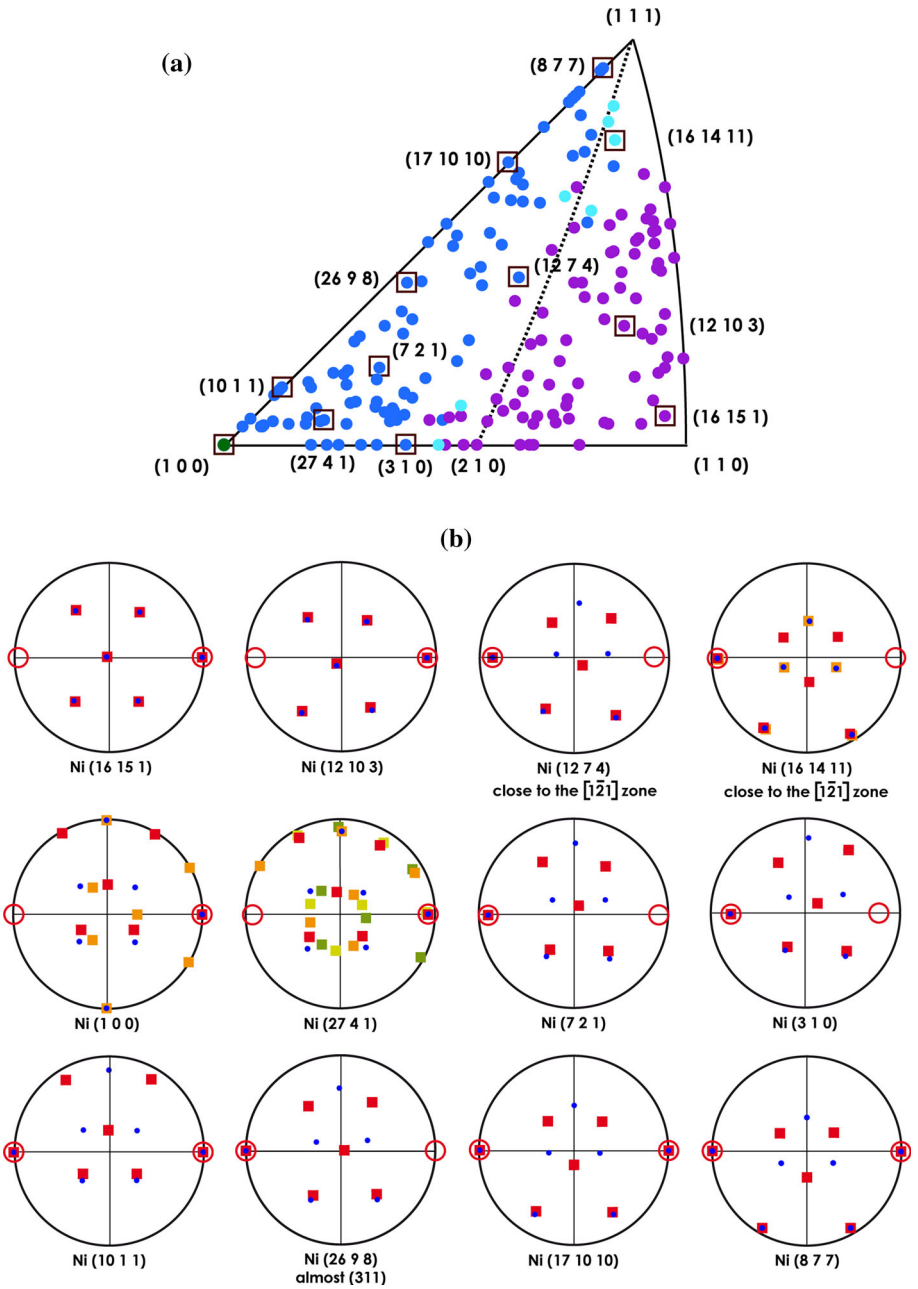

Fig. 4 **a** SST identifying the ~200 different Ni(*hkl*) substrate orientations investigated in this study. The color scheme of the *points* indicates the different ORs observed for the corresponding Ag crystals, as described in the text. The *dashed line* in the SST identifies the [1$\bar{2}$1] zone which runs from (111) to (210). *Squares* have been drawn around certain points to identify the Ni substrate orientations for which ⟨110⟩ PFs are displayed in (**b**). **b** ⟨110⟩ PFs for Ni grains of different orientations labeled by the substrate Ni(*hkl*) (*blue round symbols*) together with superimposed ⟨110⟩ PFs for the corresponding Ag crystals (*square symbols* in *red* for the most frequent ORs and in other colors for minor ORs). Only "northern hemisphere" poles are shown. Coincident Ni and Ag poles are surrounded by a *red circle*, and empty *red circles* indicate coincident Ni and Ag poles that lie in the southern hemisphere (see text) (Color figure online)

two ⟨110⟩ poles in the present experimental results is even closer than that observed in the results of the simulations. This coincidence of ⟨110⟩ poles will be discussed in detail in the "Discussion" section.

OR(C)

OR(C) is illustrated in the ⟨110⟩ PFs for the Ni(12 10 3) and Ni(16 15 1) substrate orientations in Fig. 4b. An exact Ni(110)-oriented substrate is absent from our data. The closest Ni orientation, Ni(16 15 1), is a few degrees off (110), as shown in Fig. 4a.

The experimental deviation from a precise cube-on-cube OR is shown in Fig. 5a for the Ni orientations previously identified by purple symbols in Fig. 4a. In Fig. 5a, purple symbols are reproduced from Fig. 4a, and the square red symbols identify the Ag orientations. Several corresponding pairs of Ni and Ag orientations are connected by lines to illustrate the extent of deviation from OR(C), which ranges from 0° to ~5°. The magnitudes of these experimental deviations are also generally consistent with those obtained in the simulations of the companion paper [21], and reflect tilt and/or twist misorientations about the common ⟨110⟩ direction, presumably due to the lattice

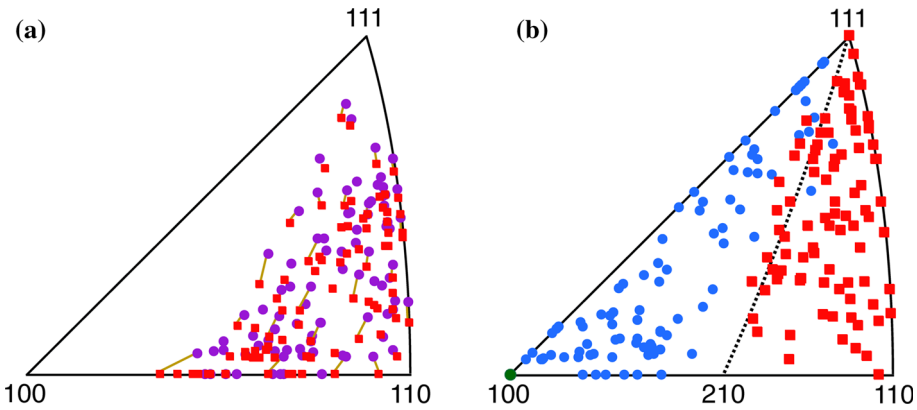

Fig. 5 **a** Ag crystal orientations (*square red symbols*) that display a cube-on-cube OR to the Ni substrate (*round purple symbols* as in Fig. 4a); **b** Ag orientations that display OR(S) (*square red symbols*) on the Ni substrate (*round blue* and *green symbols* as in Fig. 4a). The *dashed line* from (111) to (210) represents the $[1\bar{2}1]$ zone (Color figure online)

mismatch between Ni and Ag. It is worth noting that the largest deviations of the common ⟨110⟩ axes are found for the Ni surfaces which are in the vicinity of the (210).

OR(T)

OR(T) is illustrated in the ⟨110⟩ PFs of Ni(12 7 4) and Ni(16 14 11) of Fig. 4b. On these PFs, the red squares correspond to Ag with OR(T). On Ni(16 14 11), the additional orange squares correspond to Ag with OR(C) which, for this Ni substrate orientation, appears with the same frequency as OR(T). It is worth mentioning that OR(T), which occurs on many Ni substrate orientations that lie on or close to the $[1\bar{2}1]$ zone of the SST of Fig. 4a, applies to any interfacial plane along the $[1\bar{2}1]$ zone from (111) to (210). No Ni substrate orientation lying exactly on (111) was identified among the orientations investigated here. However, the Ni(8 7 7) and the Ni(16 14 11) substrate orientations, which are close to (111), can serve to extrapolate the OR to Ni(111). Thus, it is expected that the OR at Ni(111) will be OR(T) or OR(C), or a combination of both. This is consistent with the findings of the companion paper [21]. OR(T) also identifies Ag crystals that are in twin relation to other Ag crystals, in cases that are labeled as belonging to OR(C), even when they are slightly misaligned with respect to the Ni substrate. For the Ni substrate orientations shown as light blue points in Fig. 4a, OR(T) and OR(C) are present with approximately equal frequency.

OR(O)

OR(O) is illustrated in the ⟨110⟩ PF of Ni(100). The Ag crystals adopt a (111) interface plane, the in-plane ⟨110⟩ directions of which are parallel to one of the two possible ⟨110⟩ Ni directions that lie in the Ni(100) surface, i.e., there are two possible variants of the Ag orientation. One of these variants corresponds to the red squares in the ⟨110⟩ PF for the Ni(100) substrate of Fig. 4b. In addition, each variant can have a twin-related OR (orange squares). This OR is consistent with previous findings [6, 13]. In practice only one major variant is observed, because the orientation of the Ni substrate is never exactly (100) and will tend to display predominant steps along one of the two ⟨110⟩ directions that lie in the Ni(100) substrate surface. This presence of steps leads to alignment of the ⟨110⟩ steps on the Ag side of the interface, as observed in the companion paper [21]. The two possible variants and their twins appear on the ⟨110⟩ PF of Ni(27 4 1) (which is close to Ni(100)): the major variant is shown as red square symbols and the other three as orange, yellow, and green squares.

OR(S)

Examples of ⟨110⟩ PFs for the OR(S) family of ORs, which involve a gradual transition from OR(O) to OR(T), are displayed in Fig. 4b. These include Ni(10 1 1), Ni(26 9 8) (which is close to Ni(3 1 1)), Ni(17 10 10), and Ni(8 7 7), all of which lie on, or very close to, the (100)–(111) edge of the SST. Ni substrates with surfaces oriented along (27 4 1), (7 2 1), and (3 1 0) are also examples of OR(S). In these cases, the coincident ⟨110⟩ poles do not lie in the plane of the interface, but are the ⟨110⟩ poles with the smallest separation from the outer circle of the PFs, i.e., the coincident ⟨110⟩ directions lie close to the interface plane.

The experimental results for all Ag crystals which display OR(S), together with the corresponding Ni substrate orientations (i.e., those orientations shown in blue in Fig. 4a), are summarized in Figs. 5b. The figure displays the Ni orientations shown as round blue symbols (same as in Fig. 4a) together with the corresponding Ag orientations, shown as square red symbols. The Ni orientations are confined to a part of the SST with corners at (100), (111), and (210) and the corresponding Ag orientations are confined, within a few degrees, to another distinct region of the SST with corners at (111), (110), and (210), where the bold dashed line is part of the $[1\bar{2}1]$ zone.

The OR(S) family of orientations cannot readily be described by the simple types of expressions that have been used above to describe OR(C), OR(T), and OR(O). Consequently, a more complete description of OR(S) is deferred to the "Discussion" section.

Discussion

The simple orientation relationships: OR(C), OR(T), and OR(O)

The companion paper [21] has investigated the ORs that develop for Ag, on Ni substrates of 12 different orientations, by molecular dynamics simulations performed at approximately the same temperature as the annealing temperature used for the samples in the current experiments. Those simulations focused mainly on substrate orientations along the edges of the SST. In general, there is good agreement between the ORs obtained by simulations with the present experimental results. The principal discrepancy occurs in the region of orientation space, where experiments show a predominant OR(C), but where the simulations typically display both OR(C) and OR(T) in comparable proportions. This could be the result of an under-estimate of the twin boundary energy of Ag by the embedded atom method (EAM) potentials used in the simulations, since a low twin boundary energy could lead to a greater proliferation of twin-related Ag variants.

Correlation for the OR(S) on Ni substrates lying along the (100)–(111) edge of the SST

As mentioned above, the OR(S) family arises because of a transition from OR(O), where the Ag/Ni interface consists of Ag(111) parallel to Ni(100), to OR(T) where Ag(11$\bar{1}$) is parallel to Ni(111) at the interface. A correlation has been presented in the companion paper [21] to describe the evolution of this transition for Ni interface orientations along the (100)–(111) edge of the SST. This correlation predicts that as the Ni substrate orientation changes by an angle of 54.7° from (100) to (111) by rotating about [1$\bar{1}$0], the Ag orientation undergoes a change of 70.5° from (111) to (11$\bar{1}$) by rotating about [01$\bar{1}$], i.e., from the SST into the adjacent stereographic triangle. If θ is the angle between the Ni(*hkl*) interface orientation and Ni(100) along the (100)–(111) edge of the triangle, and ϕ is the angle between the Ag(*hkl*) interface orientation and Ag(111), along the (111)–(11$\bar{1}$) arc of the stereographic projection, then the correlation indicates that

$$\phi = (1 + 15.8^\circ/54.7^\circ)\theta \quad (1)$$

where the value of 15.8° (70.5°–54.7°) represents the misalignment between Ni(111) and Ag(11$\bar{1}$) when OR(O) prevails on Ni(100), and conversely, the misalignment between Ni(100) and Ag(111), when OR(T) prevails on Ni(111).

Equation 1 was found to conform to the results of the simulations of the companion paper, but a better test of that correlation can be obtained from the present experimental results, where a much greater number of Ni substrate orientations have been investigated. Figure 6 shows a comparison of the experimental values of ϕ, with the values of ϕ computed by Eq. 1. The good agreement obtained in Fig. 6 provides convincing validation for the correlation of the companion paper [21].

The correlation predicts that some of the Ag orientations that correspond to Ni substrate orientations along the (100)–(111) edge of the SST will fall in the adjacent stereographic triangle. However, to avoid any possible confusion, all Ag orientations belonging to OR(S) have been reflected back into the SST in Fig. 5b.

Finally, it should be mentioned that although it is relatively simple to construct a correlation to account for the variation of OR(S) for Ni substrate orientations that lie on the (100)–(111) edge of the SST, where one can limit consideration to only two sets of Ni and Ag interface planes, it becomes considerably more complicated to apply such a correlation to cases where OR(S) develops on Ni substrate orientations that lie within the SST.

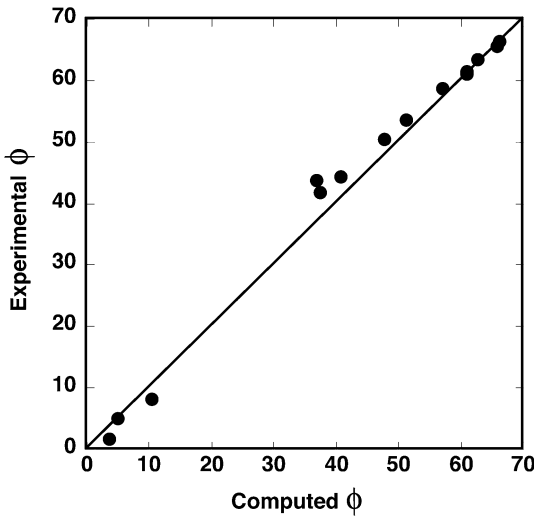

Fig. 6 Comparison of the experimental value of ϕ (the angle between Ag(*hkl*) and Ag(111) along the (111)–(11) arc of the stereographic projection) with the value of ϕ computed from the correlation of Eq. 1. The line has been added to aid the eye

OR(S) and interface step-edge alignment

The principal conclusion of the companion paper [21] is that the ORs observed in the Ag–Ni system develop as the result of an alignment at the interface of the step edges of the Ag crystals with those of the Ni substrate, which occurs during the early stages of deposition. That such alignment which also tends to lead to minimum energy interfaces has been demonstrated in a few specific cases of Ag/Ni interfaces (see companion paper [21]), but is also reasonable when considered by analogy, for example, with twist grain boundaries (GBs). In the case of symmetric twist GBs, when steps are aligned at zero twist, both the grain boundary and its energy vanish. The GB energy increases with increasing twist angle due to the formation of a dislocation array at the interface, the density of which increases with twist angle. In the case of asymmetric twist GBs, which contain a tilt component, the GB and its energy do not vanish at zero twist, and the energy increases further with increasing twist angle [24]. In the case of an A/B interface, where the lattice parameters of A and B differ, an array of interfacial dislocations already exists at zero twist angle, in order to accommodate lattice mismatch. As the twist angle increases, the crossing of steps leads to an increased density of localized distortions at step intersections that tend to increase interfacial energy [21], beyond that already present at zero twist angle (this is analogous to asymmetrical twist GBs). Thus, step alignment is also, more often than not, consistent with minimum energy interfaces in the case of A/B interfaces.

The present experimental study has investigated the ORs of Ag on Ni for many more substrate orientations than was readily feasible by computer simulations. It therefore offers an excellent opportunity to test the observation reported in the companion paper [21] that step alignment on both sides of the interface plays an important role in OR development. For that purpose, one needs to define the step-edge directions on both the Ni- and Ag-terminating surfaces at the Ag/Ni interface. This can be accomplished by making use of the terrace–ledge–kink (TLK) model of surfaces [25]. In this framework, it is first necessary to define the possible orientations of the micro-facets that can act as terraces, ledges, and kinks. This has been done here by making use of the micro-facet decomposition scheme of van Hove and Somorjai [26], in which one may pick any three micro-facets whose normals are linearly independent vectors. We choose the (111), (11$\bar{1}$), and (100) orientations because the third corner of our SST, the (110) orientation, may be viewed as being composed of (111) and (11$\bar{1}$) micro-facets.

The crystallographic direction of steps can be calculated for a given (*hkl*) interface orientation of either Ag or Ni within the SST, by a cross product of the vector normal to (*hkl*), **H**, with the vector normal to the terrace micro-facet orientation, **T**. As has been shown by van Hove and Somorjai [26], the terrace orientation of an (*hkl*) surface is given by the micro-facet containing the largest relative number of atoms, the ledge orientation is given by the micro-facet with the second relative largest number of atoms, and the kink orientation is given by the micro-facet with the smallest relative number of atoms. The relative numbers of atoms in the three types of micro-facets, N(111), N(11$\bar{1}$) and N(100) may be expressed as [26]

$$\mathrm{N}(111) : \mathrm{N}(11) : \mathrm{N}(100) = (\mathrm{k}+\mathrm{l}) : (\mathrm{k}-\mathrm{l}) : (\mathrm{h}-\mathrm{k}) \tag{2}$$

After identifying the terrace orientation by Eq. 2, the step direction, **S**, may be obtained from the cross product:

$$\mathbf{S} = \mathbf{H} \times \mathbf{T} \tag{3}$$

It should be noted that the step direction only coincides with the ledge direction when no kinks are present, i.e., when the relative number of atoms of the third ranking micro-facet in Eq. 2 is zero. This only occurs for (Ni or Ag) interface planes with orientations that belong to (100)–(111) or the (111)–(110) edges of the SST. In both of these cases, the step edges are parallel to a ⟨110⟩ direction.

As mentioned above, the EBSD data obtained from the experiments yield three Euler angles for each Ni substrate grain and its associated Ag crystallite orientations. These can be used to form the orientation matrices for Ni and Ag [27] and hence to obtain the interface (*hkl*) planes in each case. The interface planes can in turn be used to identify the step orientations by means of Eq. 3. Such an analysis has been performed for the ∼80 cases that display OR(S), since in the cases where OR(C) prevails, the steps on both sides of the interface are necessarily aligned. The results show that the steps on the Ag and Ni sides of the interface are indeed close to parallel, within an average angle of 1.0° ± 3.8°, thereby providing strong support for the importance of step alignment in OR generation observed in the companion paper [21].

OR(S) and the alignment of ⟨110⟩ directions

In "Details on the observed ORs" section, it was pointed out that the experimental results indicate a good alignment between a pair of Ni and Ag ⟨110⟩ poles, when the ⟨110⟩ directions lie either in the plane of the interface, or close to it. Indeed, there is a close connection between alignment of close-packed directions and step-edge directions, as illustrated in Fig. 7. The figure is a schematic of the top view of a high-index Ni surface that displays a kinked step, together with Ag atoms attached to the step edge. The presence of kinks on the Ni step will cause it to deviate

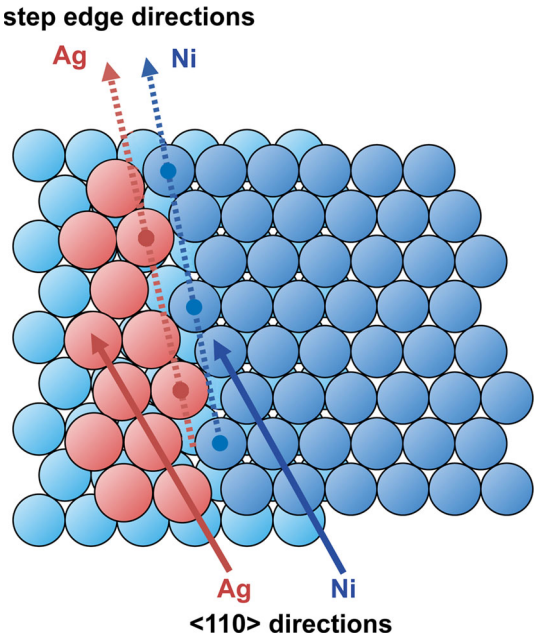

Fig. 7 Schematic top view of a step on high-index Ni surface (Ni atoms *blue*) with Ag atoms (*red*) attached to the step edge. *Dashed arrows* indicate step directions which run through the atoms at kink sites (indicated by *dots*), and *solid arrows* indicate close-packed directions (Color figure online)

from the close-packed ⟨110⟩ ledge directions. The step direction of the attached Ag atoms will generally be close to the direction of the Ni step, but will deviate somewhat due to size misfit. Since the Ni and Ag steps will consist partly of ⟨110⟩ ledge segments, the ⟨110⟩ directions in Ni and Ag will also be approximately parallel.

Final comment on OR(S)

The correlation of Eq. 1 indicates that the appropriate scaling factor for the relationship between the Ni substrate orientation along the (100)–(111) edge of the SST and the corresponding Ag orientations along the (111)–(11$\bar{1}$) arc of the stereographic projection involves an angle of 15.8°. This angle reflects the relative rotation of Ni and Ag orientations that occur in OR(S) during the transition from OR(O) to OR(T). We have computed the angle, α, between Ni(100) and the closest Ag{111} plane, as well as the angle, β, between Ni(111) and the closest Ag{111} plane, from the Euler angles that emerge from EBSD measurements, for all Ni substrate orientations which display OR(S). We find that α and β both have a range of 0 to $\sim$16°, and that the sum, $\alpha + \beta$, averages to 16.1° over the whole OR(S) family of ORs. Thus, although it has not been possible to provide an expression to describe the family of OR(S), the whole transition from OR(O) to OR(T) occurs through small adjustments in misorientation that are consistent with Eq. 1, i.e., the behavior displayed by the OR(S) for Ni substrate orientations that lie along the (100)–(111) edge of the SST.

Summary and conclusions

The ORs that develop when Ag is equilibrated on Ni substrates have been studied on polycrystalline Ni by EBSD, thereby enabling the ORs to be determined for some 200 Ni substrate orientations, uniformly distributed over orientation space. This is the first time that ORs beyond the three low-index corners of the SST have been investigated in the widely studied Ag–Ni system. The accuracy of OR measurements by EBSD has been maximized by partially dewetting the Ag film, without altering the OR, so as to allow simultaneous access by the EBSD technique to both Ag crystals and the Ni substrate. Four different types of ORs have been identified as follows: a cube-on-cube OR, a twin-related OR where the Ag orientation is either in twin relation to the substrate or to other Ag crystals, an oct-cube OR in which the Ag adopts a (111) interface plane on Ni(100), and a family of special ORs which collectively represent transitions from the oct-cube OR to the twin-related OR, under the constraint of step alignment.

The very large set of data obtained in this study supports the observation in the companion paper [21] of the pervasiveness of step alignment across the Ag/Ni interface, and thus provides strong support for its validity. The possibility that step alignment plays an important role in OR generation deserves to be tested on other classes of interfaces to determine whether it has more general validity for hetero-epitaxy in A–B systems, even when A and B have different structures or belong to different materials classes, such as metal/metal-oxide or metal/semi-conductor.

Acknowledgements The authors wish to thank Profs. W.D. Kaplan and P.A. Salvador for useful discussions, and Dr S. Bojarski for her help in the acquisition of EBSD data. The work performed at Carnegie Mellon University was supported by the MRSEC program of the National Science Foundation under Award Number DMR-0520425. ADR also wishes to acknowledge support from the Ames Laboratory (subcontract under US-DOE Contract No. DE-AC02-07CH11358).

References

1. Dregia SA, Bauer CL, Wynblatt P (1986) The structure and composition of interphase boundaries in Ni/Ag-(001) thin films doped with Au. Mater Res Soc Symp Proc 56:189–194
2. Dregia SA, Wynblatt P, Bauer CL (1987) Epitaxy for weakly interacting systems of large misfit. Mater Res Soc Symp Proc 94:111–120

3. Dregia SA, Wynblatt P, Bauer CL (1989) Computer simulations of epitaxial interfaces. Mater Res Soc Symp Proc 141:399–404
4. Gao Y, Dregia SA, Shewmon PG (1989) Energy and structure of (001) twist interphase boundaries in the Ag/Ni system. Acta Metall 37:1627–1636
5. Gao Y, Shewmon PG, Dregia SA (1989) Investigation of low-energy interphase boundaries in Ag/Ni by computer simulation and crystallite rotation. Acta Metall 37:3165–3175
6. Maurer R, Fischmeister HF (1989) Low energy heterophase boundaries in the system silver/nickel and in other weakly bonded systems. Acta Metall 37:1177–1189
7. Gao Y, Merkle KL (1990) Atomic structure of Ag/Ni interfaces. Mater Res Soc Symp Proc 183:39–44
8. Gao Y, Merkle KL (1990) High-resolution electron microscopy of metal/metal and metal/metal-oxide interfaces in the Ag/Ni and Au/Ni systems. J Mater Res 5:1995–2003
9. Gumbsch P, Daw MS, Foiles SM, Fischmeister HF (1991) Accommodation of the lattice mismatch in a Ag/Ni heterophase boundary. Phys Rev B 43:13833
10. Gumbsch P (1992) Atomistic study of misfit accommodation in cube-on-cube oriented Ag/Ni heterophase boundaries. Z Metallkd 83:500–507
11. Allameh SM, Dregia SA, Shewmon PG (1994) Structure and energy of (110) twist boundaries in the Ag/Ni system. Acta Metall Mater 42:3569–3576
12. Allameh SM, Dregia SA, Shewmon PG (1996) Energy of (110) twist boundaries in Ag/Ni and its variation with induced strain. Acta Mater 44:2309–2316
13. Floro JA, Thompson CV, Carel R, Bristowe PD (1994) Competition between strain and interface energy during epitaxial grain growth in Ag films on Ni(001). J Mater Res 9:2411–2424
14. Gumbsch P (1997) The accommodation of lattice mismatch in Ag/Ni heterophase boundaries. J Phase Equilib 18:556–561
15. Mroz S, Jankowski Z, Nowicki M (2000) Growth and isothermal desorption of ultrathin silver layers on the Ni(111) face at the substrate temperature from 180 to 900 K. Surface Sci 454:702–706
16. Chambon C, Creuze J, Coati A, Sauvage-Simkin M, Garreau Y (2009) Tilted and nontilted Ag overlayer on a Ni(111) substrate: structure and energetics. Phys Rev B 79:125412
17. Hsiao PY, Tsai ZH (2009) Huang JH, Yu GP (2009) Strong asymmetric effect of lattice mismatch on epilayer structure in thin-film deposition. Phys Rev B 79:155414
18. Chatain D, Galy D (2006) Interfaces between Pb grains and Cu surfaces. J Mater Sci 41:7769–7774
19. Krupski A, Nowicki M (2005) Investigations of Pb/Ni(111) using incident beam electron diffraction. Surface Sci 575:147–153
20. Herrmann G, Gleiter H, Biro G (1976) Investigation of low energy grain boundaries in metals by a sintering technique. Acta Metall 24:353–359
21. Wynblatt P, Chatain D (2015) Importance of interfacial step alignment in hetero-epitaxy and orientation relationships: the case of Ag equilibrated on Ni substrates. Part 1 computer simulations. J Mater Sci. doi:10.1007/s10853-015-9074-1
22. Curiotto S, Chien H, Meltzman H, Wynblatt P, Rohrer GS, Kaplan WD, Chatain D (2011) Orientation relationships of copper crystals on c-plane sapphire. Acta Mater 59:5320–5331
23. Zhang Y, Schultz AM, Li L, Chien H, Salvador PA, Rohrer GS (2012) Combinatorial substrate epitaxy: a high-throughput method for determining phase and orientation relationships and its application to $BiFeO_3/TiO_2$ heterostructures. Acta Mater 60:6486–6493
24. Wolf D (1990) Structure-energy correlation for grain boundaries in f.c.c. metals—IV. Asymmetrical twist (general) boundaries. Acta Metall Mater 38:791–798
25. Stranski IN (1928) Zur Theorie der Kristallwachstums. Z Phys Chem 136:259–277
26. van Hove MA, Somorjai GA (1980) A new microfacet notation for high-Miller-index surfaces of cubic materials with terrace, step and kink structures. Surf Sci 92:489–518
27. Rohrer GS (2001) Structure and bonding in crystalline materials. Cambridge University Press, Cambridge, p 72